CHEMISTRY OF MATERIALS

ARTICLE

pubs.acs.org/cm

Biomimetic Self-Assembling Copolymer–Hydroxyapatite Nanocomposites with the Nanocrystal Size Controlled by Citrate

Y.-Y. Hu, X. P. Liu, X. Ma, A. Rawal, T. Prozorov, M. Akinc, S. K. Mallapragada, and K. Schmidt-Rohr*

Ames Laboratory, Ames, Iowa 50011, United States

Supporting Information

ABSTRACT: Citrate binds strongly to the surface of calcium phosphate (apatite) nanocrystals in bone and is thought to prevent crystal thickening. In this work, citrate added as a regulatory element enabled molecular control of the size and stability of hydroxyapatite (HAp) nanocrystals in synthetic nanocomposites, fabricated with self-assembling block copolymer templates. The decrease of the HAp crystal size within the polymer matrix with increasing citrate concentration was documented by solid-state nuclear magnetic resonance (NMR) techniques and wide-angle X-ray diffraction (XRD), while the shapes of HAp nanocrystals were determined by transmission electron microscopy (TEM). Advanced NMR techniques were used to characterize the interfacial species and reveal enhanced interactions between mineral and organic matrix, concomitant with the size effects. The surface-to-volume ratios determined by NMR spectroscopy and long-range $^{31}P\{^{1}H\}$ dipolar dephasing show that 2, 10, and 40 mM citrate changes the thicknesses of the HAp crystals from 4 nm without citrate to 2.9, 2.8, and 2.3 nm, respectively. With citrate concentrations comparable to those in body fluids, HAp nanocrystals of sizes and morphologies similar to those in avian and bovine bones have been produced.

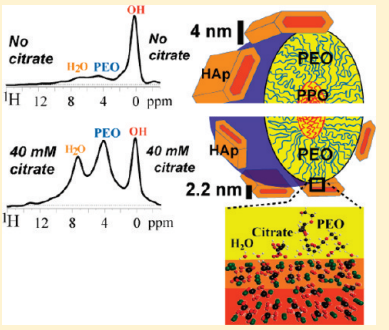

KEYWORDS: bioinspired materials, biocompatibility, bone, crystal control, hybrid materials, nuclear magnetic resonance

INTRODUCTION

Bone, the primary supporting and protective organ of the mammalian body, is a nanocomposite of nanosized carbonated apatite crystals and the fibrous protein collagen (ca. 40 vol % each), with smaller contributions from other proteins and water.[1−5] The integration of the stiff apatite nanocrystals within the tough collagen fibers renders bone lightweight yet strong and tough. Human bone undergoes constant dynamic remodeling to repair fatigue damage, such as microcracks induced by stress.[6] However, when the damage is beyond the self-restoring ability of bone and severely compromises the quality of life especially in the elderly, therapeutic approaches to regenerate the mineralized tissues are desired. Ideal materials employed in tissue repair therapies should exhibit structural features similar to those in bone, be biocompatible, biodegradable, and bioactive.

Various strategies of tissue engineering have been developed in recent years.[7] Cell- or protein-based methods simulate the mineralization process in bone,[8−11] but the limited availability of materials, immunogenic responses, potential disease transmission, or interference with the therapeutic process curtails their application.[7] Nonproteinaceous biopolymers, including cellulose, chitosan, and gelatin, have been also employed, but these have fewer apatite-nucleating functional groups such as carboxylate or phosphate moieties, and their properties are not readily tunable. Therefore, the use of synthetic polymers has been an attractive option to provide a scaffold for apatite formation and introduce apatite nucleating reagents. Polymers or polypeptides with acidic groups are favorable in inducing the precipitation of apatite and have been investigated extensively.[12]

A balance between mechanical properties and bioactivity should be considered in biomaterials science; composites of synthetic polymer and calcium phosphate provide a favorable combination. Among various synthesis schemes intended to mimic bone,[13] a bottom-up sol−gel method using inorganic ionic precursors and self-assembling polymers is advantageous since it can control the structure at the molecular level while inducing some hierarchical ordering as seen in bone.[14] With this method, our group has successfully demonstrated the synthesis of organic and inorganic self-assembling nanocomposites using Pluronic (polyethylene oxide−polypropylene oxide triblock copolymer) and its derivatives, polymers coupled to apatite-nucleating peptides, and $K_{170}L_{30}$ diblock copolypeptides as templates that precipitate apatite nanocrystals within the organic matrix.[15−17] Progress has been made to more closely mimic the structure of bone; for instance, hydroxyapatite has been stabilized, and the inorganic content has been increased from 15 wt % to over 50 wt %, compared to 65 wt % in bone. Similar research has been pursued by other groups. For instance, Pramanik and Kar synthesized thermoplastic apatite-poly(ether etherketone) nanocomposites,[18] Song et al. used cross-linked polymethacrylamide and polymethacrylate hydrogels to template the formation of HAp nanoparticles,[19] and poly(lactic acid), poly(glycolic acid), and

Received: February 11, 2011
Revised: March 22, 2011
Published: April 12, 2011

poly(ε-caprolactone)/HAp composites have also been constructed for their biodegradability.[20] However, although organic−inorganic nanocomposites have been fabricated, the regulation of the apatite crystal size and morphology has not been discussed. Nevertheless, the crystal dimensions, particularly the crystal thickness, are critical to the mechanical properties of bone, in that a thickness of ∼3 nm prevents the propagation of cracks.[21] Also, recent research implied that desirable osteoconductivity could be achieved with synthetic HAp resembling bone minerals in composition, size, and morphology.[22]

Many studies of bone biomineralization have focused on identifying proteins promoting or inhibiting the apatite crystal formation, such as a series of Glx-proteins.[5] It has been hypothesized that proteins such as osteocalcin have a mechanism for mineral surface recognition which allows for biological control of the mineral crystal growth.[23] However, a most recent close examination of the interface between collagen and apatite crystals in bone by advanced solid-state NMR techniques[24] has revealed that citrate, a small molecule, is the dominant organic molecule there, tightly bound to apatite and covering the surface with a density of one citrate molecule per 4 nm^2 (ca. $^1/_6$ of the available area). About 80 wt % of the total citrate in the body is accumulated in bone. Carboxylate groups are key for regulating the formation of apatite,[5,25] and citrate in bone provides more carboxylate groups than all the proteins other than collagen taken together. In vitro studies have shown that citrate at higher concentrations results in smaller HAp nanocrystals.[26,27] Moreover, citrate stabilizes HAp over other phosphates[28] and synthetic materials pretreated with citrate give better biocompatibility in tissue repair.[29,30] Despite these studies, the effect of citrate upon the local molecular composition and surface structure is not well understood. This is in part due to the challenge of selectively characterizing mineral surfaces, especially those buried in organic matrices. The surface- and structure-directing effect of small molecules is general to a wide variety of functionally important materials such as zeolites,[31] mesoporous materials,[32] and sol−gel based electronic materials,[33] in addition to biomaterials.

Inspired by the study of citrate−apatite in bone and in vitro, we have added citrate as a third component in our synthesis of self-assembled Pluronic polymer and HAp nanocomposites. This research allows more precise control over the crystal size and morphology of synthetic HAp within a polymer matrix in order to more closely mimic the structure and morphology of nanocrystals in bone. By adjusting the concentration of citrate, we have achieved molecular control over the size of the HAp nanocrystals within the Pluronic polymer matrix. These synthetic nanocomposites have been characterized by transmission electron microscopy (TEM), X-ray diffraction (XRD), small angle neutron scattering (SANS), and advanced solid-state nuclear magnetic resonance (NMR) techniques. Multinuclear NMR can provide detailed information on the composition and nanometer-scale structure of synthetic and biological calcium phosphate nanoparticles.[34−37] ^{31}P NMR has been used for molecular characterization of the calcium phosphate species formed, to probe molecular proximities on the nanometer scale, and to accurately quantify the surface and core phosphate contents of the nanocrystals. $^1H-^{31}P$ heteronuclear correlation (HetCor) spectra with ^1H spin diffusion provides a powerful method to monitor the formation of organic−inorganic nanocomposites and qualitatively reveal the enhanced surface area of HAp with increasing citrate concentration. $^1H-^{31}P$ HARDSHIP NMR[38] has been used to quantitatively determine the crystal size and compare with that in bone, which is often considered the ideal biocomposite. The results obtained from NMR and XRD show how the apatite nanocrystal size decreases with increasing citrate concentration. The citrate concentration was set comparable to that in body fluids to determine whether apatite nanocrystals similarly sized as in natural bone can be generated. TEM has been applied to reveal the morphologies of apatite nanocrystals with varying citrate concentrations, while small angle neutron scattering (SANS) can determine the effect of citrate and HAp nanocrystal formation on the long-range order and morphology of the Pluronic polymer matrix assembly. It is expected that the biocompatibility of biosynthetic materials can be enhanced by the incorporation of citrate within the nanocomposites to produce similarly structured HAp nanocrystals as in bone apatite.

EXPERIMENTAL SECTION

Chemicals. The Pluronic F127 block copolymer, poly(ethylene oxide)-b-poly(propylene oxide)-b-poly(ethylene oxide) (PEO-PPO-PEO), was purchased from Sigma Aldrich (St. Louis, MO). Its average molecular weight is about 12.6 kDa. An aqueous solution of the polymer can self-assemble into micelles at low temperature and concentration,[14] and transform to a viscous gel upon increase in temperature (typically above 25 °C) or concentration. All the other chemicals in this study were purchased from Sigma Aldrich or Fisher Scientific, and used without further purification.

Nanocomposite Synthesis. The calcium phosphate nanocomposites were prepared using self-assembling polymers as templates as follows: 0.01 mol of $Ca(NO_3)_2$ was dissolved in 10 mL of 30 wt % Pluronic F127 solution at 4 °C, followed by addition of 0.2 mL of ammonium citrate at various concentrations and mixed for 2 h at 4 °C. Two mL of 3 M $(NH_4)_2HPO_4$ was then added. The sample was brought to room temperature and allowed to form a gel with gentle stirring. NH_4OH was then added to adjust the pH to 7.5−8; the pH was checked and readjusted to 7.5−8 after 24 h and beyond until it remained stable. Four hydrogel samples with citrate concentrations of 0, 2, 10, and 40 mM were prepared. The samples were freeze-dried and characterized.

In addition, samples were washed to remove free polymer and ammonium nitrate, as needed for characterization. The sample powder was suspended in pure water, centrifuged, and the supernatant was removed. This procedure was repeated three times to minimize the amount of residual free polymer and ammonium nitrate.

Characterization. *XRD.* The structure of the freeze-dried and washed samples was investigated by XRD (X′Pert PRO, PANalytical Inc., Westborough, MA,) and analyzed by X′pert Data Collector. The diffractometer was operated at 45 kV and 40 mA. CuKα radiation with a wavelength of 0.15418 nm was employed. The scan rate was 0.021°/s with a step size of 0.017° over the range of $10° \leq 2\theta \leq 60°$.

TEM. Imaging of the samples was performed without staining with the Tecnai G^2 F20 Scanning Transmission Electron Microscope (STEM) (FEI Company, Hillsboro OR) equipped with High Angle Annular Dark Field (HAADF) and Energy Dispersive X-ray Spectroscopy (EDS) detectors at an operating voltage of 200 kV. Twenty microliters of a suspension of the sample was dispersed in 2 mL of distilled H_2O. A drop of the diluted suspension was placed on a holey carbon-supported copper grid. Multiple areas of each sample were examined to determine the average size of the particles in the nanocomposites, both in bright field TEM mode and in STEM mode.

SANS. Small-angle neutron scattering (SANS) was used to highlight the structure of the Pluronic block copolymer in the nanocomposite gels. One mL of deuterium oxide (D_2O) was added to about 0.5 mL of gel sample. The polymer phase has higher neutron scattering contrast than

the inorganic phase in a deuterated solvent, since the scattering length of ^{1}H is negative while the scattering lengths of all other isotopes involved are positive and of similar magnitude.

The experiments were performed using the 30 m small angle scattering instrument on beamline NG7 at the National Center for Neutron Research, National Institute of Standards and Technology (NIST), Gaithersburg, MD. A cold neutron source with an average wavelength of 6 Å was used. The samples were sealed in quartz cylindrical cells with a 1-mm path length. The scattered neutrons were detected by a two-dimensional detector with three different sample-to-detector distances of 13, 4, and 1 m. The scattering vector, q, was varied between 0.004 Å^{-1} < q < 0.56 Å^{-1}, where $q = (4\pi/\lambda)\sin\theta$, in which λ is the neutron wavelength and θ is half the scattering angle. The $I(q)$ data were placed on an absolute scale in units of cm^{-1}. Data reduction and plots were accomplished by using SANS reduction and analysis macros provided by NIST (http://www.ncnr.nist.gov/programs/sans/data/red_anal.html).[39]

NMR. All the NMR experiments were carried out on a Bruker Biospin DSX-400 spectrometer (Bruker-Biospin, Rheinstetten, Germany) at 400 MHz for ^{1}H, 162 MHz for ^{31}P, and 100 MHz for ^{13}C. A Bruker 4-mm double resonance magic-angle spinning (MAS) probehead was used with spinning frequencies of 4.3 kHz for ^{1}H−^{31}P HetCor and ^{31}P spin diffusion experiments and 6.5 kHz for other ^{31}P experiments. The 90° pulse length was 4 μs for ^{1}H, and 4.5 μs for ^{31}P and ^{13}C.

A 200 s recycle delay was used in direct-polarization ^{31}P NMR experiments without or with two rotor periods of gated ^{1}H−^{31}P heteronuclear recoupling. The two-pulse phase-modulation (TPPM) ^{1}H−^{31}P heteronuclear decoupling strength was 60 kHz during ^{31}P detection. Hartman-Hahn cross-polarization (CP) of 1 ms was employed for experiments requiring polarization transfer from ^{1}H to ^{31}P or ^{13}C. ^{13}C NMR spectra were acquired after cross-polarization from ^{1}H and total suppression of sidebands (TOSS), at ν_r = 5.3 kHz, with a 1-s recycle delay and 6700 scans per spectrum. ^{1}H−^{31}P HetCor experiments were carried out with MREV-8 for ^{1}H−^{1}H homonuclear decoupling and ^{1}H chemical shifts were scaled by 0.47 accordingly during data processing. One hundred sixty t_1 increments of 60 μs were employed and multiecho detection[40] was implemented to enhance signal sensitivity. In ^{31}P spin diffusion experiments, a short CP contact time of 0.1 ms was employed to generate ^{31}P magnetization selectively in phosphates close to protons with subsequent 0.1-ms and 1-s ^{31}P spin diffusion times.[15] A spin diffusion time of 100 s was used in a sample without citrate and containing two phosphate phases. The duration of the z-period was incremented in 8 steps of $t_r/8$ = 29.1 μs in order to cancel dispersive contributions to the spinning sidebands, which would result in baseline distortions. ^{1}H−^{31}P HARDSHIP experiments[38] were performed with direct polarization and recoupling times of 0.3, 0.6, 0.9, 2.1, 3.0, 4.6, 6.1, 7.7, and 9.2 ms. Differential T_2 relaxation of surface and core phosphate signals in S_0 was corrected for as outlined in ref 38. The NIST hydroxyapatite ^{1}H peak at 0.18 ppm and ^{31}P peak at 2.8 ppm was used to calibrate ^{1}H and ^{31}P chemical shifts, respectively.

Avian and bovine bones used in HARDSHIP experiments were extracted from the midsections of femur bones from a mature hen and a 4-year-old cow. The surface was cleaned with a scalpel to remove muscle tissue and then washed with a solution of methanol and chloroform to remove lipids. The bone was ground to a powder and lyophilized to remove any traces of solvent and bulk water.

■ RESULTS AND DISCUSSION

The properties of synthetic nanocomposites are strongly dependent on the mineral size, composition, and the surface structure as well as its interaction with the surrounding organic matrix. Mineralization of an organic matrix increases the mechanical strength provided that the mineral is distributed

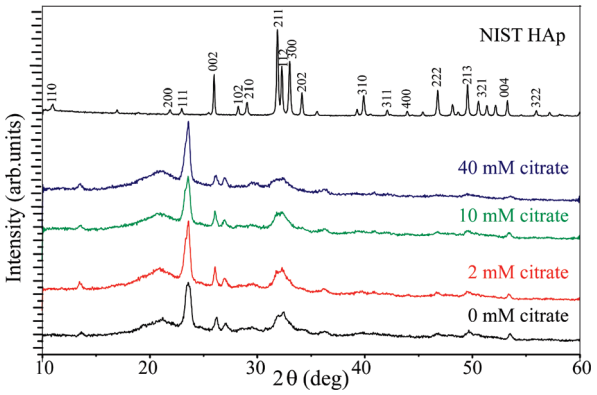

Figure 1. XRD patterns of Pluronic polymer−hydroxyapaite nanocomposite samples with different citrate concentrations after freeze-drying. The diffraction pattern of NIST HAp is shown for reference.

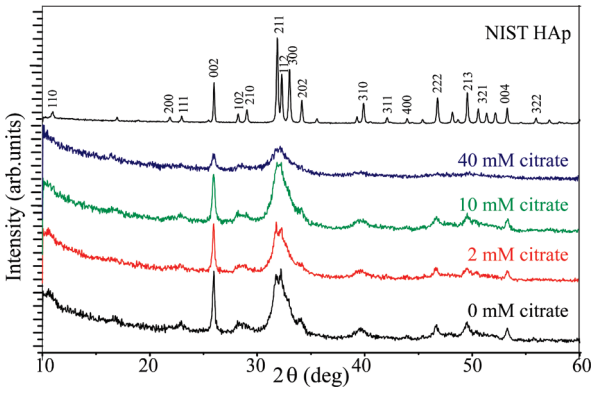

Figure 2. XRD patterns of Pluronic polymer−hydroxyapatite nanocomposites after washing. The diffraction pattern of NIST HAp is shown for reference.

uniformly and has molecular-level interactions with the templating organic matrix. XRD, TEM, SANS, and NMR are a powerful set of complementary techniques that yield information about the size of the mineral nanocrystals as well as the effect of mineralization on the structure of the templating organic polymer. 1D and 2D NMR techniques uniquely enable selective molecular characterization of the nanocrystal surface and core, as well as the mineral−organic interactions, from which insights about the influence of citrate and formation of the nanocomposites can be obtained.

XRD. XRD patterns of the four synthesized samples after freeze-drying and after washing are shown in Figures 1 and 2, respectively. When compared to the pure NIST hydroxyapatite (HAp) pattern, the patterns show similarities and differences. The peaks in the diffraction pattern, in particular the intense bands at approximately 2θ = 32° and 2θ = 26°, confirm that the mineralized phase is predominantly HAp. Although the patterns of the synthesized materials differ from those of NIST HAp in showing much broader peaks, they are very similar to those of human bone and dentin.[41] The broad peak at approximately 2θ = 32° is a composite band contributed from three of the most intense peaks of HAp [(211), (112), and (300) planes].[15] These broad peaks are indicative of the formation of HAp crystals in the low nanometer thickness range. Additional diffraction peaks seen in Figure 1 at 2θ = 21° and 2θ = 24° were assigned to crystalline

dx.doi.org/10.1021/cm200355n |*Chem. Mater.* 2011, 23, 2481–2490

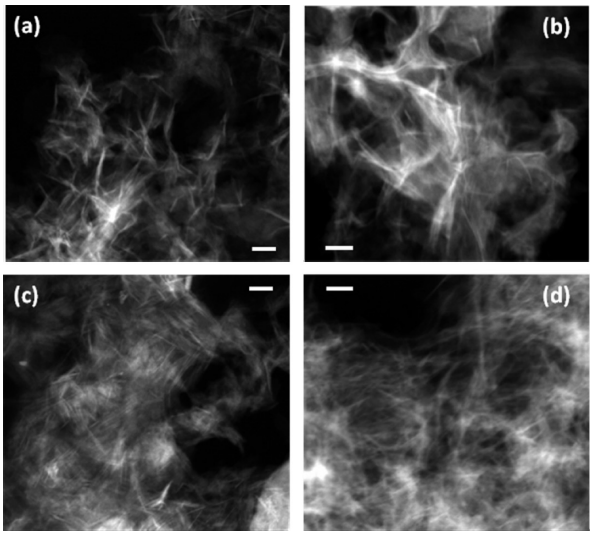

Figure 3. HAADF-STEM images of hydroxyapatite nanocrystals fabricated within a Pluronic polymer matrix using different citrate concentrations: (a) 0 mM; (b) 2 mM; (c) 10 mM; (d) 40 mM. All scale bars are 50 nm.

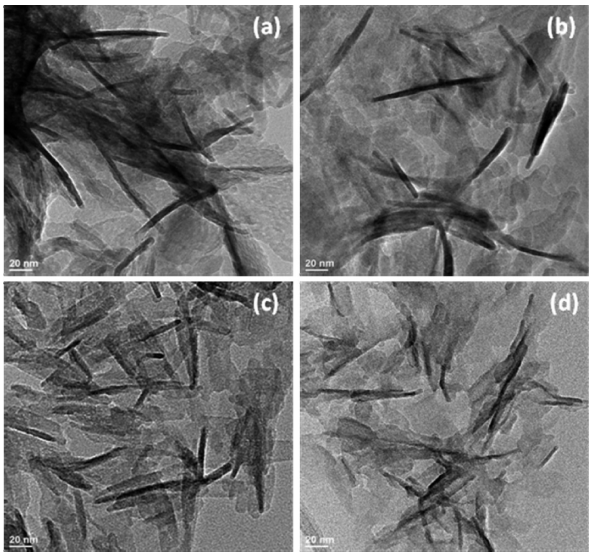

Figure 4. Bright-field TEM images of hydroxyapatite nanocrystals fabricated within a Pluronic polymer matrix using different citrate concentrations: (a) 0 mM; (b) 2 mM; (c) 10 mM; (d) 40 mM. The magnification is 88 000, and scale bars are 20 nm.

polyethylene oxide[17] which was confirmed by the much reduced intensity of these two peaks after removal of the polymer by washing (see Figure 2). Most importantly, it is seen from Figure 2 that as the concentration of citrate in the synthesis was increased, the diffraction peaks broadened, which indicates that the size of the HAp nanocrystals is decreased. This is consistent with the NMR results, as discussed in more detail below.

TEM. HAADF-STEM is sensitive to scattered electrons generated in proportion to the atomic number (Z) of the atoms in the specimen. It can be used for obtaining compositional and morphological information of a sample (Z-contrast imaging), where contrast varies roughly as a function of Z^2.[42,43] It is, therefore, possible to image high-Z species inside a densely populated lower-Z environment of a nanocomposite specimen. Example of such analysis of the unwashed hydroxyapatite samples is shown in Figure 3. Dark-field (DF) images are obtained with HAADH-STEM at a magnification of 110 000. Here the bright spots correspond to the calcium-rich thicker areas of the nanocomposite. According to Figure 3, the sample prepared with the highest concentration of citrate has the shortest and thinnest particles.

Figure 4 shows bright-field (BF) transmission electron micrographs obtained at a magnification of 88 000. Analysis both in the BF TEM mode and HAADF-STEM mode reveals elongated particles of approximately 5 nm thickness and a mean particle length of 50 nm. These data are in good agreement with the results from the other techniques.

SANS. Figure 5 shows SANS data in a plot of log $I(q)$ vs log (q) for Pluronic polymer− hydroxyapatite nanocomposite gels with different citrate concentrations. Due to the small neutron scattering contrast between D_2O and calcium phosphate, whose isotopes all have positive scattering lengths of similar magnitudes, the inorganic component is essentially invisible here. This enables selective observation of the structure of the polymer micelles. For all four samples, a pronounced peak is observed at essentially the same q_{max} of 3 A^{-1}, which corresponds to a characteristic length scale of ca. 15 nm. This peak was observed previously for the neat hydrated Pluronic material and shown to be due to the self-organization of the triblock copolymer into micelles.[17] The fact that the observed scattering pattern is very similar for the different samples indicates that the nanocrystals as well as the citrate molecules are incorporated into the organic matrix in a manner that does not disrupt the self-assembled structure of the pluronic polymer micelles.

NMR Characterization of the Synthetic Composites. Direct-polarization (DP) 1D solid state ^{31}P NMR spectra yield quantitative site populations of the different phosphate species precipitated in the mineral phase. Figure 6 shows the ^{31}P DP NMR spectra of composites synthesized with Pluronic polymer, calcium phosphate, and citrate of different concentrations (bold line). Analysis of spectra reveals two overlapping spectral components that are recognizable in all four samples, which correspond to two different phosphate species.[36] The first is represented by a relatively sharp peak resonating at ∼2.8 ppm, characteristic of orthophosphate (PO_4^{3-}) in hydroxyapatite (HAp). 2D $^1H-^{31}P$ HetCor NMR further proves it to be from HAp by its connection to the $OH^{-1}H$ resonance, as described below. The second phosphate species exhibits a broad peak centered around 2 ppm and with a full width at half-maximum (fwhm) of 5 ppm, indicating a disordered phosphate environment. The NMR signal of the phosphate species near protons (^1H) can be selectively enhanced by $^{31}P\{^1H\}$ cross-polarization (CP). The CP spectra (Figure S1 in the Supporting Information) of the samples show lineshapes different from those in the DP ^{31}P spectra due to this selective enhancement. In Figure S1 the signal of the disordered phosphate component is selectively enhanced over that of the HAp phosphate species. This indicates that the disordered phosphate component has a closer proximity to ^1H than the HAp component.[36]

On the other hand, based on the difference in their distance from the surface and polymer protons (which exhibit strong spin−spin interactions and therefore a short spin−spin relaxation time T_2), the two phosphate components can be separated by $^1H-^{31}P$ HARDSHIP NMR experiments, in which ^{31}P signal of the disordered phosphate is dephased (suppressed) by protons with short T_2 much faster than that of HAp.[38] This

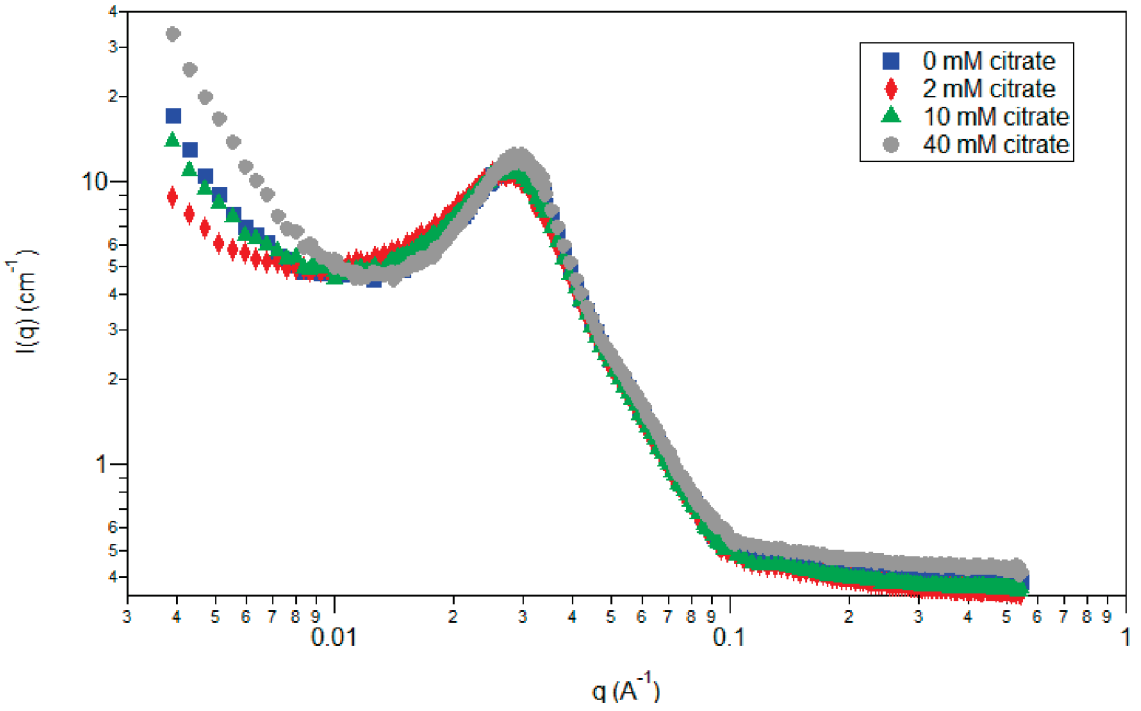

Figure 5. SANS curves of Pluronic−hydroxyapatite nanocomposites fabricated using different citrate concentrations.

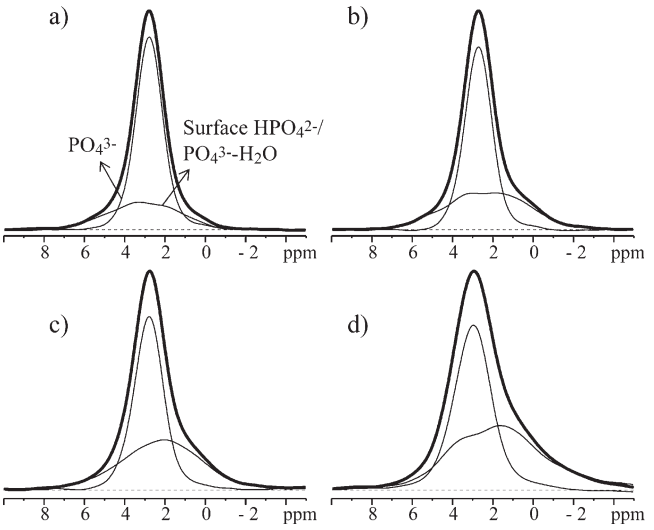

Figure 6. Direct polarization (DP) ^{31}P NMR spectra of composites synthesized with Pluronic polymer, calcium phosphate, and with ammonium citrate of different concentration: (a) 0 mM citrate, (b) 2 mM citrate, (c) 10 mM citrate, and (d) 40 mM citrate. The spectra have been deconvoluted into a relatively sharp peak, obtained experimentally after long ^{31}P{^{1}H} HARDSHIP dephasing of surface phosphates by polymer or surface protons and assigned to the hydroxyapatite core of the nanocrystals, and a remaining broad component of surface PO_4^{3-}/PO_4^{3-}−H_2O. Magic angle spinning frequency: ν_r = 6.5 kHz.

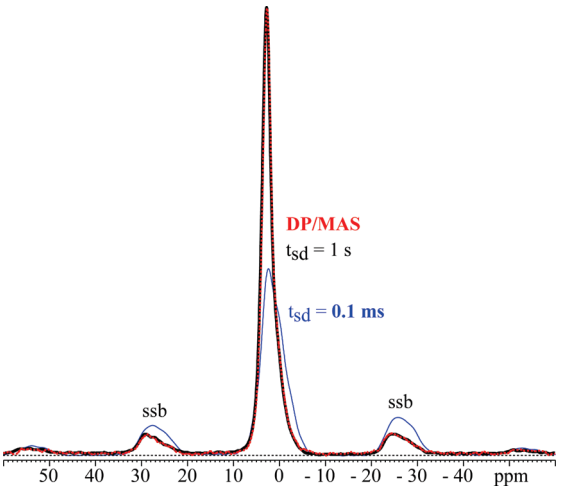

Figure 7. ^{31}P NMR spectra of the Pluronic polymer−HAp composite with 40 mM citrate. Cross-polarization (CP) ^{31}P NMR spectra with short contact time of 0.1 ms and ^{31}P spin diffusion time of 0.1 ms (thin blue line) and 1 s (thick black line) are compared. The direct-polarization spectrum (dashed red line, nearly indistinguishable from the 1-s spectrum) is used as a reference to gauge the completion of spin diffusion. Spinning sidebands are labeled as "ssb". ν_r = 4.3 kHz.

differential dephasing enables a deconvolution of the overlapping DP spectra of the two phosphate components into two separate components as shown in Figure 6 (thin lines).

Proximity of Phosphate Components. The molecular proximities between different ^{31}P components in the nanocomposite can be probed by ^{31}P spin diffusion.[15,37] In the spin diffusion process, the ^{31}P magnetization is stored along the z axis, and is then distributed to nearby nuclei via dipolar couplings. This method allows us to evaluate proximities among the different phosphate species on the 2-nm scale. First, the magnetization is selectively placed on the ^{31}P nuclei of the broad component by short (0.1 ms) cross-polarization from protons (Figure 7, thick line); then via the ^{31}P−^{31}P spin diffusion process, the magnetization spreads to the nearby ^{31}P nuclei. After 1 s of spin diffusion, the whole spectrum (Figure 7, thin line) matches the DP spectrum

dx.doi.org/10.1021/cm200355n |*Chem. Mater.* 2011, 23, 2481–2490

Table 1. Composition of Phosphates Formed in Pluronic Polymer and HAp Nanocomposites with Different Citrate Concentrations Quantified Based on the Deconvolution of the DP Spectra[a]

citrate concentration	core PO_4^{3-}	surface HPO_4^{2-} and PO_4^{3-}—H_2O	estimated crystal thickness from surface fraction (±0.5 nm)	estimated crystal thickness HARDSHIP NMR (±20%)	$B_{1/2}$ (radian) of (310) peaks from XRD of washed samples	estimated crystal diameter from X-ray diffraction (±15%)
0 mM	73%	27%	4.4 nm	3.5 nm	0.03 (7 ± 5)	4.0 nm
2 mM	59%	41%	2.9 nm	2.7 nm	0.06 (1 ± 7)	2.4 nm
10 mM	57%	43%	2.8 nm	2.6 nm	0.06 (3 ± 7)	2.3 nm
40 mM	48%	52%	2.3 nm	2.2 nm	0.1 (0 ± 2)	1.5 nm

[a] The estimated HAp crystal thicknesses based on the ratio of surface phosphates (HPO_4^{2-} and PO_4^{3-}—H_2O) and the total phosphates are also listed and compared with the thicknesses obtained from HARDSHIP NMR and calculated by applying the Debye—Scherrer formula to the (310) peak in the wide-angle X-ray diffraction patterns of the washed samples. The uncertainties of the thickness values are also specified.

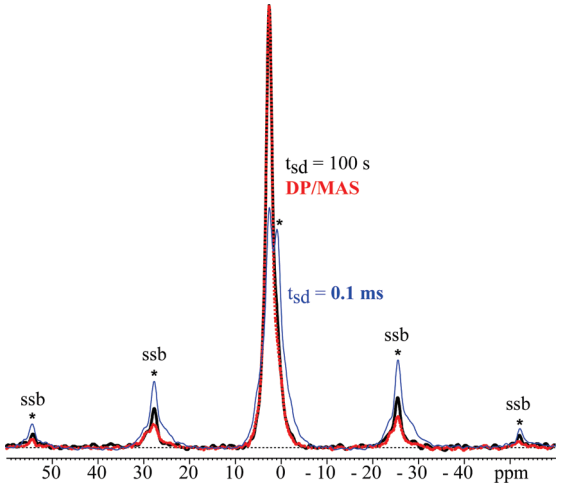

Figure 8. ^{31}P NMR spectra of a Pluronic polymer and calcium phosphate composite with 0 mM citrate. Cross-polarization (CP) ^{31}P NMR spectra with short contact time of 0.1 ms and ^{31}P spin diffusion times of 0.1 ms (thin blue line) and 100 s (thick black line) are compared. The direct-polarization spectrum (dashed red line) is used as a reference to gauge the completion of spin diffusion. Spinning sidebands are labeled as "ssb", and the sharp centerband and sidebands of the nonapatitic phase are labeled by asterisks. ν_r = 4.3 kHz.

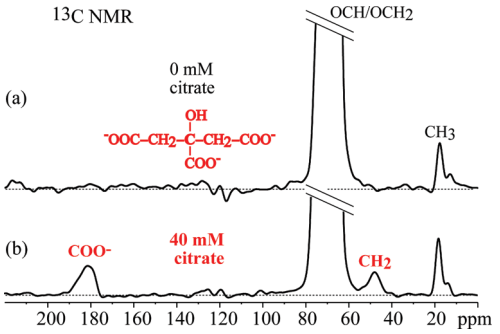

Figure 9. ^{13}C CP/MAS NMR spectra of composites of Pluronic polymer and calcium phosphate synthesized with (a) 0 and (b) 40 mM ammonium citrate.

(Figure 7, dotted line), indicating that spin diffusion equilibrium is reached. The fact that spin diffusion occurs from the disordered to the HAp phosphate indicates that these two components are not macroscopically phase separated. Indeed, the observed fast 1-s time scale of the ^{31}P spin diffusion between these two kinds of phosphates reveals that they are in close proximity on the 2-nm length scale. Therefore, the disordered component resonating at 2 ppm, which is close to surface H_2O (HPO_4^{2-}/PO_4^{3-}—H_2O) as well as the HAp phosphate species, must be the surface layer of the HAp nanocrystals, which is similar to the structure in native bone.

Quantification of Surface HPO_4^{2-}/PO_4^{3-}—H_2O and Core PO_4^{3-}. Quantification of surface and core phosphates of the synthetic HAp in each sample enables monitoring the influence of citrate on the molecular structure of the precipitating mineral phase. This is done by integrating the two components in the deconvoluted DP spectra in Figure 6. The results in Table 1 show that as the citrate concentration is increased from 0 to 40 mM, the amount of surface HPO_4^{2-}/PO_4^{3-}—H_2O species nearly doubles from 27% to 52%, while the core PO_4^{3-} content concomitantly decreases from 73% to 48%, which indicates that the specific surface area of the nanocrystals increases. In other words, the addition of citrate results in smaller HAp crystals. In particular, at a citrate concentration of 2 mM, similar to the average citrate concentration in body fluids, 59% core PO_4^{3-} and 41% surface HPO_4^{2-}/PO_4^{3-}—H_2O are produced, which is very similar to the fractions seen in chicken bone, where 65% is core PO_4^{3-} and 35% surface HPO_4^{2-}/PO_4^{3-}—H_2O. The tuning of nanocrystal size and surface fraction is expected to have important consequences for their solubility behavior and the mineral—organic interaction.

Stabilization of HAp by Citrate. Repeated syntheses of all samples mentioned above were analyzed to evaluate the reproducibility of the results. Syntheses with ammonium citrate as an ingredient always yielded HAp, while without citrate, sometimes other phosphate phases were found to form, which indicates that citrate uniquely stabilizes HAp crystals over other calcium phosphates and does so effectively at very small crystal thicknesses. This is consistent with the citrate-induced destabilization of phases such as brushite and their conversion into HAp.[28] To give an example of a non-HAp phosphate resulting from one of our syntheses without citrate, Figure 8 shows the ^{31}P CP/MAS spectrum with 0.1 ms contact time (thick line). It consists of two phosphate components; one is nanocrystalline HAp with core PO_4^{3-} resonating at 2.8 ppm and a broad band of surface HPO_4^{2-}/PO_4^{3-}—H_2O. The other resonates at 1.3 ppm with strong spinning sidebands, which is the signature of a local PO_4 environment with strong deviations from tetrahedral symmetry. ^1H—^{31}P HetCor spectra show that this 1.3-ppm ^{31}P correlates with ^1H resonating around 10 ppm (POH) and H_2O with strong hydrogen bonding at 7 ppm (Figure S2). Both

dx.doi.org/10.1021/cm200355n |*Chem. Mater.* 2011, 23, 2481–2490

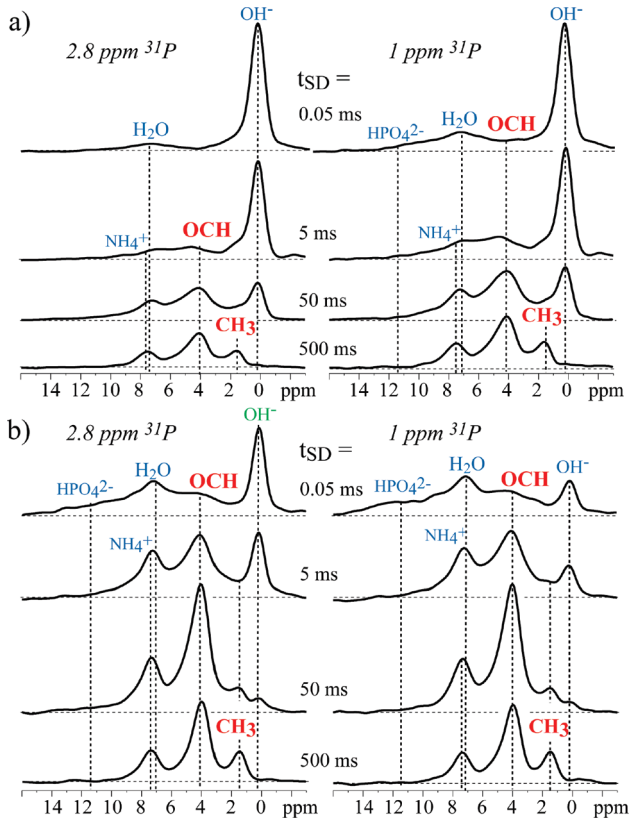

Figure 10. ^{1}H spectra from cross sections taken at 2.8 and 1.0 ppm ^{31}P of 2D ^{1}H−^{31}P HetCor NMR spectra of composites synthesized with Pluronic polymer, calcium phosphate, and (a) 0 mM, and (b) 40 mM ammonium citrate. The ^{1}H spin diffusion times t_{SD} are 0.05, 5, 50, and 500 ms.

^{31}P and ^{1}H spectra are typical of HPO_4^{2-} surrounded by bound H_2O. ^{31}P spin diffusion in Figure 8 (thin line) shows proximity only of surface HPO_4^{2-}/PO_4^{3-}−H_2O and core PO_4^{3-} of HAp. Even after 100 s of spin diffusion, the CP spectrum (thin line) does not match the DP spectrum (dashed line); note in particular the lack of sideband equilibration and mismatch of the right shoulder of the centerband. This indicates that in this sample, some of the HPO_4^{2-} with ^{31}P resonating at 1.3 ppm is a phase distinct from HAp and these two phosphates are separated on the >2-nm scale. In the presence of citrate, such non-HAp phases were not observed.

^{13}C NMR of Bound Citrate. Detection of the bound citrate itself is possible in ^{13}C NMR. Figure 9 compares cross-polarization ^{13}C NMR spectra of the composites with 0 and 40 mM citrate. Signals at 48 and 181 ppm appearing in the citrate-containing sample must be assigned to the CH_2 and COO^- groups of citrate, respectively,[24] while the signal of the central quaternary C−OH carbon of citrate expected near 76 ppm is hidden by overlap with the strong peak of PEO. The large width of the lines is characteristic of apatite-bound citrate,[24] while crystalline citrate shows much sharper peaks, with widths of less than 1 ppm.[24]

^{1}H Spectra of Phosphate Environments. The ^{1}H−^{31}P HetCor spectra with ^{1}H homonuclear decoupling and minimal ^{1}H spin diffusion time of 0.05 ms (Figure 10, top row) reveal the immediate proton environment around specific ^{31}P, which helps confirm the identity of the various phosphates. The ^{1}H spectra

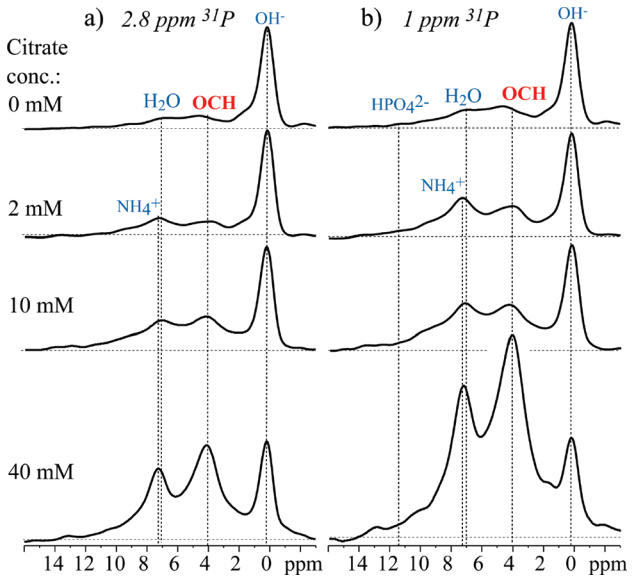

Figure 11. ^{1}H spectra from cross sections of 2D ^{1}H−^{31}P HetCor NMR spectra with 5 ms of ^{1}H spin diffusion in composites of Pluronic polymer and calcium phosphate synthesized with 0, 2, 10, or 40 mM ammonium citrate. ^{1}H spectra were taken at (a) 2.8 ppm ^{31}P and (b) 1.0 ppm ^{31}P. The height of the OH^- peak at 0.2 ppm has been normalized for convenience of comparison.

extracted at 2.8 ppm of ^{31}P of the sample containing 0 mM citrate (Figure 10a, left column, top row) exhibit predominantly the OH^- proton peak at 0.2 ppm; this confirms the assignment of the 2.8 ppm peak in the ^{31}P spectra to HAp. The relatively weak ^{1}H peak at ∼7 ppm is from bound water at the surface of HAp. The ^{1}H spectrum (Figure 10a, right column, top row) taken at 1 ppm of ^{31}P to minimize the interference from HAp represents the ^{1}H environment of the disordered phosphate component. It shows reduced intensity of the OH^- peak and increased intensity of the bound water signal (more distinctively seen in Figure 10b, top row). Furthermore, we see additional intensity at ∼11 ppm and ∼4 ppm, belonging to surface HPO_4^{2-} and organic OCH_2 species, respectively. In particular, the signal for the OCH_2 species from the hydrophilic PEO segments of the Pluronic polymer confirms that the disordered phosphate is the surface component of the HAp nanocrystal. The relatively broad OCH_2 peak indicates that the PEO segments are immobilized due to favorable interactions with the mineral surface, potentially mediated by hydrogen bonding. This indicates formation of an intimately mixed nanocomposite system.

Nanocomposite Formation. The formation of the nanocomposite is proved most convincingly by monitoring the ^{1}H spin diffusion from polymer protons to the mineral phase in 2D ^{1}H−^{31}P HetCor experiments.[14] With increasing ^{1}H spin diffusion time, the presence of the polymer OCH_2 (4 ppm) and CH_3 (1.5 ppm) peaks in the ^{1}H−^{31}P HetCor experiments (Figures 10 and S3, t_{SD} = 5, 50, and 500 ms) proves that in all four samples the mineral is in nanometer-scale contact with the organic matrix. The addition of citrate enables formation of crystals that are so small that even after a short ^{1}H spin diffusion time of only 0.05 ms, the OCH_2 proton peak at 4 ppm is observed, proving contact between the inorganic phosphate and Pluronic polymer. This is most apparent in Figure 10b for the nanocomposite synthesized with the highest citrate concentration (40 mM). At

dx.doi.org/10.1021/cm200355n |Chem. Mater. 2011, 23, 2481–2490

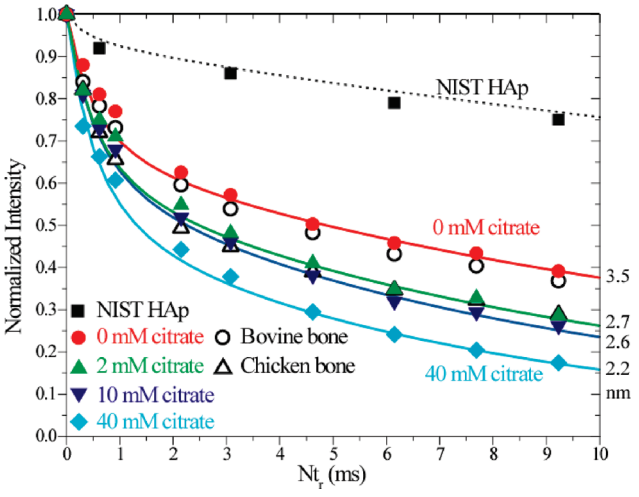

Figure 12. $^{31}P\{^1H\}$ HARDSHIP dephasing in composites of Pluronic polymer and calcium phosphate, synthesized with 0, 2, 10, and 40 mM ammonium citrate. NIST HAp is used as a reference of the decay only due to protons within the crystal lattice. Bovine bone and chicken bone are used to compare the crystal size of synthetic NIST hydroxyapatite and apatite in bones. Error margins are comparable to the size of the symbols. Solid lines are simulated dephasing curves to obtain the thicknesses of crystals. The simulation procedure has been detailed in ref 38.

longer spin diffusion times, one can see the ^1H peak at 1.3 ppm, from CH_3 of the hydrophobic PPO segments at the core of the Pluronic block-copolymer micelles appear. At the same spin diffusion times, magnetization has arrived from the relatively mobile OCH_2/OCH of PEO and PPO, and NH_4^+ of the starting material $(NH_4)_2HPO_4$, whose signals appear at 4 ppm and 7.3 ppm, respectively. This is balanced by a decrease in the relative intensity of the OH^- and HPO_4^{2-} signals at 0.2 and 11 ppm, respectively. Equilibrium of the magnetization between HAp and Pluronic polymer, evidenced by similar relative peak intensities in all ^1H cross sections, is reached within 500 ms ^1H spin diffusion in all samples. ^1H spectra taken at 1 ppm ^{31}P exhibit faster spin diffusion to polymer protons than those taken at 2.8 ppm, which again confirms that the disordered phosphate component is at the organic−inorganic interface.

Nanocrystal Size. The size of the nanocrystals is crucial to the overall performance and properties of nanocomposite materials. In the present syntheses, it is also a measure of the specific molecular interactions of citrate with the mineral phase, whereby it promotes and more importantly stabilizes the HAp phase at a few nanometer thickness. The rate of ^1H spin diffusion from the organic protons to the mineral matrix, observed in a series of $^1H-^{31}P$ HetCor spectra, reveals that spin diffusion between the organic and inorganic protons is faster as the citrate concentration is increased from 0 to 40 mM. This indicates that on average, the mineral has a larger surface area in contact with the organic phase in the 40 mM citrate sample than at lower citrate concentrations. This means that the average nanocrystal size decreases as more citrate is added. This trend is seen most clearly in a comparison of spectra from all samples after 5 ms of ^1H spin diffusion (Figure 11). With the intensities of the OH^- peaks scaled to equal height, the spin diffusion rate can be gauged by the intensity of the polymer ^1H peaks, in particular the OCH_2/OCH at 4 ppm. The sample with 40 mM citrate shows the most intense OCH_2/OCH peak and thus the fastest ^1H spin diffusion and therefore the smallest HAp crystals, followed by the samples with 10, 2, and then 0 mM citrate. The faster spin diffusion also implies more extensive interactions between mineral and polymer matrix, which is favorable to the stability of the nanocomposite.

The 2D HetCor experiments with spin-diffusion provide a direct comparative but qualitative measurement of the nanocrystal size. More quantitative measurements of the surface-to-volume ratio of the mineralized HAp nanocrystals in these samples were carried out using $^1H-^{31}P$ HARDSHIP experiments.[38] In these experiments, the ^{31}P magnetization is dephased (destroyed) in a selective manner mostly by polymer and surface protons (Figure 12). The faster the measured dephasing, the larger the surface-to-volume ratio and the smaller the crystals. The measurement shows that increasing the citrate concentration decreases the synthetic HAp crystal size within the polymer matrix. The dephasing behavior of the sample with 2 mM citrate is similar to that of avian bone. This is compatible with the average citrate concentration of ∼2−3 mM in body fluid and tissues in chicken.[44] The HARDSHIP dephasing of bovine bone is only slightly faster than that of synthetic HAp made with 0 mM citrate, consistent with a citrate concentration of ∼0.08 mM in bovine blood.[45]

The thickness of HAp nanocrystals can be estimated from (i) the results of $^1H-^{31}P$ HetCor experiments with ^1H spin diffusion; (ii) the surface and core fractions derived from deconvoluted DP spectra; (iii) the width of the (310) peak in X-ray diffraction; and (iv) the $^{31}P\{^1H\}$ HARDSHIP signal decay. In principle, the ^1H spin diffusion time required to reach equilibrium in $^1H-^{31}P$ HetCor experiments can be used to estimate the thickness of the inorganic domain, but this requires knowledge of spin diffusion coefficients and ^1H densities in the organic and inorganic layers. Nevertheless, even without these parameters available, the thickness of apatite crystals can still be approximately evaluated based on the similar synthetic systems in our previous published results. All the samples discussed in this paper exhibit faster spin diffusion than the Pluronic30-8 sample[17] made with Pluronic polymer and calcium phosphate salt without citrate under similar experimental conditions, which was characterized by various techniques, including wide-angle X-ray diffraction, solid-state NMR, small angle neutron/X-ray scattering (SANS/SAXS), and TEM, and in which the thickness of the HAp crystals is ∼4.8 nm. Therefore, the thickness of the HAp crystals in all the samples in this paper is <5 nm.

With a surface phosphate layer of $d_s \approx 0.4$-nm thickness, the typical aspect ratio of crystals in bovine bone[46,47] and the surface-to-volume ratio of apatite crystals, the crystallite thickness d of the four synthetic samples presented in this paper can be estimated based on

$$\text{Fraction of surface } HPO_4^{2-} \text{ and } PO_4^{3-} = d_s \times (\text{surface/volume})$$
$$= d_s \times 2 \times (L \times W + L \times d + W \times d)/(L \times W \times d) \quad (1)$$

For long thin crystals, eq 1 simplifies to $S/V \approx 2/d$. Since the length (L) and width (W) of the crystals are not infinite, a more accurate estimate needs to consider changes in length and width of HAp crystals. Assuming a fixed aspect ratio of d:W:L = 1:3:6, we have $S/V = 3/d$ according to eq 1 and the crystal thicknesses of the synthetic HAp range between 2.3 and 4.4 nm, as listed in Table 1.

dx.doi.org/10.1021/cm200355n |Chem. Mater. 2011, 23, 2481–2490

For comparison, the HAp crystal diameters have also been estimated by applying the Debye−Scherrer equation

$$d = K\lambda/(B_{1/2}\cos\theta) \quad (2)$$

to the (310) X-ray diffraction peak of the washed samples synthesized with different citrate concentrations, where K is chosen as 0.9, λ = 0.154 nm is the X-ray wavelength, $B_{1/2}$ is the full width at half-maximum (fwhm) of the diffraction peak, and θ = 20° is half the diffraction angle of the (310) peak. The crystal thicknesses calculated from X-ray diffraction, see Table 1, are somewhat smaller than those estimated from the phosphate compositions. This can be attributed to the disordered surface layers (>0.6 nm thickness combined) that may not contribute to the coherent scattering.

Analysis of $^{31}P\{^1H\}$ HARDSHIP NMR data by curve fitting[38] as shown in Figure 12 gives crystal thicknesses between 3.5 and 2.2 nm, again for d:W:L = 1:3:6 and with 2 × 0.3 nm of surface layers beyond the surface phosphorus layers. The ^1H transverse relaxation time in the simulations was T_2 = 0.6 ms, and the ^1H density of the polymer phase, $1/(0.29\ \text{nm})^3$. The thickness values obtained from HARDSHIP, listed in Table 1, are similar to those from the surface-to-volume ratio.

Our data show no indications of a broad distribution of crystallite thicknesses. The various crystallites in each micrograph of Figure 4 show similar thicknesses, and the Bragg peaks in the XRD patterns of Figure 2 seem to have a fairly homogeneous envelope, rather than broad and narrow components from small and large crystallites, respectively. The fairly good agreement in the thickness values obtained by different methods is also an indication of a fairly narrow thickness distribution. Finally, the broadening of the narrow component in the ^{31}P NMR spectra of Figure 6 with decreasing crystal thickness indicates that the cores of most crystallites are subject to more disorder as the crystallites get thinner; this rules out the assignment of that narrow component to a set of thick crystals.

Mechanism of Apatite Crystal Size Reduction by Citrate. The three carboxyl groups of citrate have pK_a values of 3.1, 4.8, and 6.4, therefore, at pH =7.5−8, they are completely ionized and can bind strongly to Ca^{2+} on the HAp surface. In studies of citrate in natural bone[23] or of citrate interacting with HAp in vitro,[26,27,29,48] citrate is found on the surface of apatite crystals without being incorporated within the crystal lattice, due to the relatively larger size of citrate molecules compared with lattice ions, such as phosphate or OH^-; this indicates that once a citrate molecule occupies a certain surface area of growing apatite, the further crystal growth on top of that area will be terminated unless the citrate molecule departs. In addition, surface-bound citrate molecules generate a negatively charged surface area,[26] which repels negatively charged phosphate ions, thus inhibiting further crystal growth. Via electrostatic repulsion, the negatively charged apatite surface also prevents the aggregation of the primary crystallites into bigger particles.[26]

CONCLUSIONS

The molecular species, their relative concentrations, and the proximity of different inorganic and organic components in synthesized bone-mimicking nanocomposites have been assessed by a full complement of NMR, diffraction, and electron microscopy techniques. Our data show that the addition of citrate in the bottom-up synthesis of self-assembled Pluronic polymer and HAp nanocomposites enables molecular control over the growth of the apatite crystal size, similar to that in native bone. The combination of XRD and $^1H-^{31}P$ NMR techniques show that citrate is able to stabilize HAp crystals of extremely small thickness (2 nm, ∼3 unit cells), over other calcium phosphate species. The mineralization of the organic matrix occurs without disturbing the supramolecular structure of the polymer gel, as documented by the nearly unchanged SANS patterns with and without citrate. The crystal size of HAp can be fine-tuned on the nanometer scale by varying the citrate concentration. By using concentrations of citrate similar to those in body fluid, we have successfully produced apatite nanocrystals that mimic those in natural bone. The increase in citrate concentrations to 40 mM makes the HPO_4^{2-}/PO_4-H_2O surface species the dominant fraction of the mineral phase, as determined by careful analysis of quantitative ^{31}P NMR spectra. The presence of citrate and the structural similarity of the synthetic HAp nanocrystals with bone apatite may contribute to better biocompatibility of these nanocomposites.

ASSOCIATED CONTENT

Supporting Information. Figures with cross-polarization ^{13}C NMR spectra and cross sections from $^1H-^{31}P$ HetCor spectra. This material is available free of charge via the Internet at http://pubs.acs.org.

AUTHOR INFORMATION

Corresponding Author
*E-mail: srohr@iastate.edu.

ACKNOWLEDGMENT

This work was supported by the U.S. Department of Energy, Office of Basic Energy Science, Division of Materials Sciences and Engineering. The research was performed at the Ames Laboratory. Ames Laboratory is operated for the U.S. Department of Energy by Iowa State University under Contract DE-AC02-07CH11358. Thanks to Dr. Jennifer O'Donnell (Iowa State University) for helping to perform the SANS experiments, and to Dr. Bosiljka Njegic for help with the TOC figure.

REFERENCES

(1) Buckwalter, J. A.; Glimcher, M. J.; Cooper, R. R.; Recker, R. *J. Bone Joint Surg. Am.* **1995**, *77A*, 1256.
(2) Rey, C.; Combes, C.; Drouet, C.; Glimcher, M. J. *Osteoporos. Int.* **2009**, *20*, 2155.
(3) Weiner, S.; Traub, W. *FASEB J.* **1992**, *6*, 879.
(4) Weiner, S.; Wagner, H. D. *Annu. Rev. Mater. Sci.* **1998**, *28*, 271.
(5) Zhu, W.; Robey, P. G.; Boskey, A. L. In *Osteoporosis*; Marcus, R., Feldman, D., Nelson, D., Rosen, C. J., Eds.; Elsevier Academic Press: San Diego, CA, 2008; Vol. 1.
(6) Wasserman, N.; Brydges, B.; Searles, S.; Akkus, O. *Bone* **2008**, *43*, 856.
(7) Palmer, L. C.; Newcomb, C. J.; Kaltz, S. R.; Spoerke, E. D.; Stupp, S. I. *Chem. Rev.* **2008**, *108*, 4754.
(8) Cui, F. Z.; Li, Y.; Ge, J. *Mater. Sci. Eng., R* **2007**, *57*, 1.
(9) Heath, C. A. *Trends Biotechnol.* **2000**, *18*, 17.
(10) Landis, W. J.; Silver, F. H.; Freeman, J. W. *J. Mater. Chem.* **2006**, *16*, 1495.
(11) Salgado, A. J.; Coutinho, O. P.; Reis, R. L. *Macromol. Biosci.* **2004**, *4*, 743.
(12) Shin, H.; Jo, S.; Mikos, A. G. *Biomaterials* **2003**, *24*, 4353.
(13) Vallet-Regi, M. *C. R. Chim.* **2010**, *13*, 174.

(14) Enlow, D.; Rawal, A.; Kanapathipillai, M.; Schmidt-Rohr, K.; Mallapragada, S.; Lo, C. T.; Thiyagarajan, P.; Akinc, M. *J. Mater. Chem.* **2007**, *17*, 1570.
(15) Hu, Y. Y.; Yusufoglu, Y.; Kanapathipillai, M.; Yang, C. Y.; Wu, Y. Q.; Thiyagarajan, P.; Deming, T.; Akinc, M.; Schmidt-Rohr, K.; Mallapragada, S. *Soft Matter* **2009**, *5*, 4311.
(16) Kanapathipillai, M.; Yusufoglu, Y.; Rawal, A.; Hu, Y. Y.; Lo, C. T.; Thiyaigarajan, P.; Kalay, Y. E.; Akinc, M.; Mallapragada, S.; Schmidt-Rohr, K. *Chem. Mater.* **2008**, *20*, 5922.
(17) Yusufoglu, Y.; Hu, Y.; Kanapathipillai, M.; Kramer, M.; Kalay, Y. E.; Thiyagarajan, P.; Akinc, M.; Schmidt-Rohr, K.; Mallapragada, S. *J. Mater. Res.* **2008**, *23*, 3196.
(18) Pramanik, S.; Kar, K. K. Apatite-poly(ether etherketone) nano composites: prosthesis materials: SBF-conditioned study. *65th Annual Technical Conference-Society of Plastics Engineers*; **2007**, pp 2558−2562.
(19) Song, J.; Malathong, V.; Bertozzi, C. R. *J. Am. Chem. Soc.* **2005**, *127*, 3366.
(20) Armentano, I.; Dottori, M.; Fortunati, E.; Mattioli, S.; Kenny, J. M. *Polym. Degrad. Stab.* **2010**, *95*, 2126.
(21) Gao, H. J.; Ji, B. H.; Jager, I. L.; Arzt, E.; Fratzl, P. *Proc. Natl. Acad. Sci. U. S. A.* **2003**, *100*, 5597.
(22) Gay, S.; Arostegui, S.; Lemaitre, J. *Mater. Sci. Eng., C* **2009**, *29*, 172.
(23) Hoang, Q. Q.; Sicheri, F.; Howard, A. J.; Yang, D. S. C. *Nature* **2003**, *425*, 977.
(24) Hu, Y. Y.; Rawal, A.; Schmidt-Rohr, K. *Proc. Natl. Acad. Sci. U. S. A.* **2010**, 22425.
(25) Sato, K.; Kumagai, Y.; Tanaka, T. *J. Biomed. Mater. Res.* **2000**, *50*, 16.
(26) Martins, M. A.; Santos, C.; Almeida, M. M.; Costa, M. E. V. *J. Colloid Interface Sci.* **2008**, *318*, 210.
(27) Lopez-Macipe, A.; Gomez-Morales, J.; Rodriguez-Clemente, R. *Adv. Mater.* **1998**, *10*, 49.
(28) Jiang, W. G.; Chu, X. B.; Wang, B.; Pan, H. H.; Xu, X. R.; Tang, R. K. *J. Phys. Chem. B* **2009**, *113*, 10838.
(29) Hempel, U.; Reinstorf, A.; Poppe, M.; Fischer, U.; Gelinsky, M.; Pompe, W.; Wenzel, K. W. *J. Biomed. Mater. Res., Part B* **2004**, *71B*, 130.
(30) Schneiders, W.; Reinstorf, A.; Pompe, W.; Grass, R.; Biewener, A.; Holch, M.; Zwipp, H.; Rammelt, S. *Bone* **2007**, *40*, 1048.
(31) Burton, A. W. *J. Am. Chem. Soc.* **2007**, *129*, 7627.
(32) Taguchi, A.; Schuth, F. *Microporous Mesoporous Mater.* **2005**, *77*, 1.
(33) Reisfeld, R.; Saraidarov, T. *Opt. Mater.* **2006**, *28*, 64.
(34) Cho, G.; Wu, Y.; Ackerman, J. L. *Science* **2003**, *300*, 1123.
(35) Kaflak-Hachulska, A.; Samoson, A.; Kolodziejski, W. *Calcif. Tissue. Int.* **2003**, *73*, 476.
(36) Jäger, C.; Welzel, T.; Meyer-Zaika, W.; Epple, M. *Magn. Reson. Chem.* **2006**, *44*, 573.
(37) Huang, S.-J.; Tsai, Y.-L.; Lee, Y.-L.; Lin, C.-P.; Chan, J. C. C. *Chem. Mater.* **2009**, *21*, 2583.
(38) Schmidt-Rohr, K.; Rawal, A.; Fang, X. W. *J. Chem. Phys.* **2007**, *126*, 054701/1.
(39) Kline, S. R. *J. Appl. Crystallogr.* **2006**, *39*, 895.
(40) Hou, S. S.; Beyer, F. L.; Schmidt-Rohr, K. *Solid State Nucl. Magn. Reson.* **2002**, *22*, 110.
(41) Liao, S.; Watari, F.; Uo, M.; Ohkawa, S.; Tamura, K.; Wang, W.; Cui, F. Z. *J. Biomed. Mater. Res., Part B.* **2005**, *74B*, 817.
(42) Muller, S. A.; Engel, A. *Chimia* **2006**, *60*, A749.
(43) Sousa, A. A.; Hohmann-Marriott, M.; Aronova, M. A.; Zhang, G.; Leapman, R. D. *J. Struct. Biol.* **2008**, *162*, 14.
(44) Hertelendy, F.; Taylor, T. G. *J. Bone Joint Surg. Br.* **1963**, *45*, 220.
(45) Thunberg, T. *Physiol. Rev.* **1953**, *33*, 1.
(46) Fratzl, P.; Schreiber, S.; Klaushofer, K. *Connect. Tissue Res.* **1996**, *35*, 9.
(47) Tong, W.; Glimcher, M. J.; Katz, J. L.; Kuhn, L.; Eppell, S. J. *Calcif. Tissue Int.* **2003**, *72*, 592.
(48) Rhee, S. H.; Tanaka, J. *Biomaterials* **1999**, *20*, 2155.